ACS OMEGA

http://pubs.acs.org/journal/acsodf

Article

In Situ X-ray Absorption Spectroscopy of PtNi-Nanowire/Vulcan XC-72R under Oxygen Reduction Reaction in Alkaline Media

Joesene Soto-Pérez,* Luis E. Betancourt, Pedro Trinidad, Eduardo Larios, Arnulfo Rojas-Pérez, Gerardo Quintana, Kotaro Sasaki, Christopher J. Pollock, Louise M. Debefve, and Carlos R. Cabrera*

Cite This: *ACS Omega* 2021, 6, 17203−17216

Read Online

ACCESS | Metrics & More | Article Recommendations | Supporting Information

ABSTRACT: Studying the oxygen reduction reaction (ORR) in the alkaline electrolyte has proven to promote better catalytic responses and accessibility to commercialization. Ni-nanowires (NWs) were synthesized via the solvothermal method and modified with Pt using the spontaneous galvanic displacement method to obtain PtNi-NWs. Carbon Vulcan XC-72R (V) was used as the catalyst support, and they were doped with NH_3 to obtain PtNi-NWs/V and PtNi-NWs/V−NH_3. Their electrocatalytic response for the ORR was tested and PtNi-NWs/V provided the highest specific activity with logarithmic values of 0.707 and 1.01 (mA/cm^2_{Pt}) at 0.90 and 0.85 V versus reversible hydrogen electrode (RHE), respectively. PtNi-NWs showed the highest half-wave potential ($E_{1/2}$ = 0.89 V) at 1600 rpm and 12 $\mu g_{Pt}/cm^2$ in 0.1 M KOH at 25.00 ± 0.01 °C. Additionally, the catalysts followed a four-electron pathway according to the Koutecký−Levich analysis. Moreover, durability experiments demonstrated that the PtNi-NW/V performance loss was like that of commercial Pt/V along 10,000 cycles. Electrochemical ORR *in situ* X-ray absorption spectroscopy results showed that the Pt L_3 edge white line in the PtNi-NW catalysts changed while the electrochemical potential was lowered to negatives values, from 1.0 to 0.3 V versus RHE. The Pt/O region in the *in situ* Fourier transforms remained the same as the potentials were applied, suggesting an alloy formation between Pt and Ni, and Pt/Pt contracted in the presence of Ni. These results provide a better understanding of PtNi-NWs in alkaline electrolytes, suggesting that they are active catalysts for ORR and can be tuned for fuel cell studies.

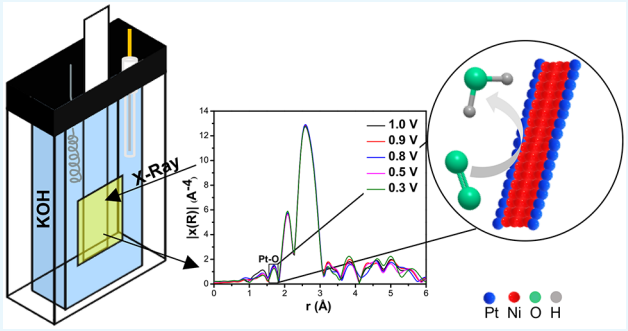

1. INTRODUCTION

Fossil fuels have been the primary source of energy generation for decades. Their continuous consumption is linked to an increase in greenhouse gas pollutants which is related to global warming. Advances in technology are essential to replace our current fuel dependency.[1] Proton exchange membrane fuel cells (PEMFCs) and anion exchange membrane fuel cells (AEMFCs) powered by hydrogen can potentially fulfill these demands at a lower environmental cost.[2] Fuel cells (FCs) could replace the internal combustion engine and revolutionize the vehicle industry reducing the abundance of gaseous emissions such as CO_2. Alternate vehicles powered by batteries are an option, but they need long hours of recharging, and FCs excel with shorter times to resupply their fuel.[3] An ongoing challenge to extend FCs into a broader range of applications is to increase their performance while reducing the cost of manufacturing. Catalyst materials can reduce the cost of the FC assembly; thus, researchers are attempting to improve their chemical constitution and chemical structure without sacrificing the performance activity.

Platinum (Pt) is by far the most studied material used for FC applications because it can be used for both hydrogen evolution reaction (HER) at the anode and oxygen reduction reaction (ORR) at the cathode.[4] Pt establishes a challenge for the mass production of FCs, and it is an expensive material. To use FCs as daily drivers for automotive purposes and sustain all the industry demands, less expensive catalysts should be considered. To comply, researchers have adopted strategies by modifying the catalyst structure, morphology, and/or incorporating less expensive foreign materials or metal oxides. Some of the approaches taken by several groups are using Pt/C catalysts,[5] core−shell nanoparticles,[6−8] nonprecious metals,[9,10] and nanowires (NWs).[11−14] The main importance is that these materials achieve high current densities and increase normalized mass activities for the ORR.[15]

If we use different catalysts for the HER and the ORR in the FCs, we could reduce their cost. However, in PEMFCs, less expensive materials are limited, oxides are unstable, and mainly noble metals are the active elements. Additionally, the ORR has

Received: February 18, 2021
Accepted: June 15, 2021
Published: July 1, 2021

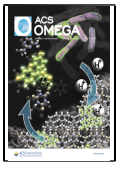

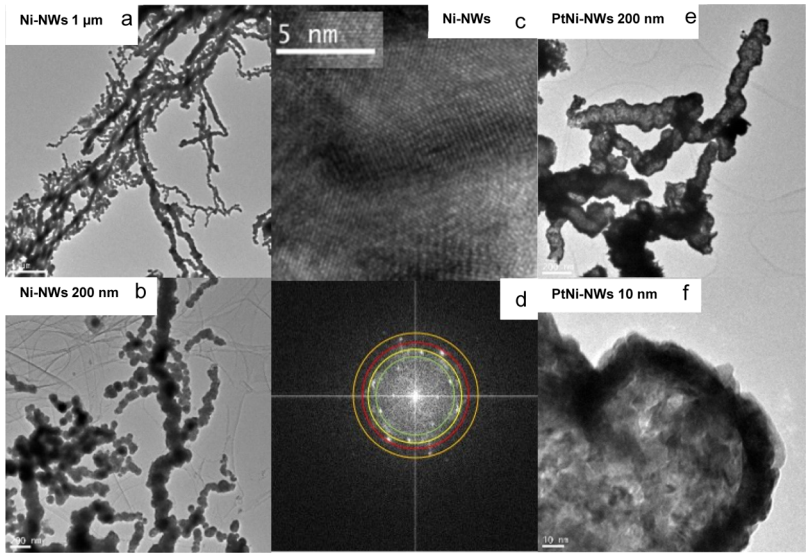

Figure 1. TEM images of Ni-NWs and PtNi-NWs. (a,b) Bright-field (BF) images of Ni showing wire-like morphology. (c) High-resolution image of the Ni-NWs. (d) FFT spots of the Ni-NWs. (e,f) BF images of PtNi-NWs.

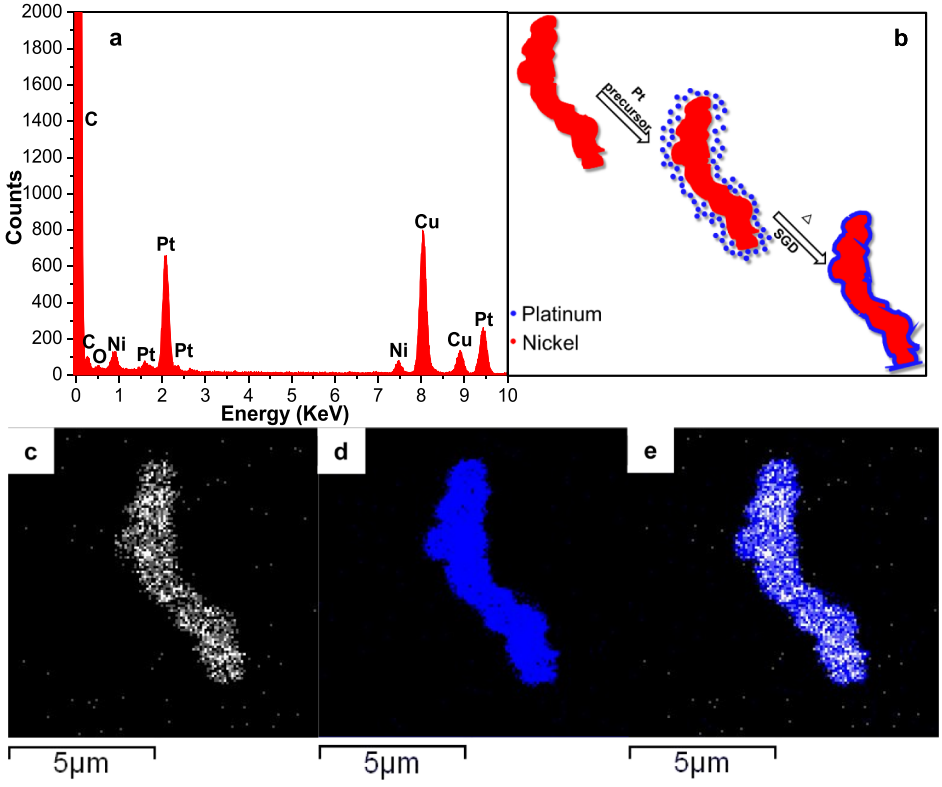

Figure 2. EDS spectrum of the PtNi-NWs (a). Suggested diagram for the atom positioning in the NW (b). X-ray map of the PtNi-NW sample, nickel (c), platinum (d), and overlay of PtNi (e).

a sluggish behavior at a low pH.[16] An alternate route is to operate an FC at a higher pH (using an alkaline electrolyte). In alkaline environments, oxides are stable and other non-noble metals can undertake the ORR.

More than a decade ago, studies by Markovic *et al.* found that $Pt_3Ni(111)$ is 10 and 90 times more active for ORR than the Pt(111) and Pt/C catalyst, respectively.[17] Improvements of PtNi catalysts are still under development. If Pt remains as the active material for ORR, researchers must minimize the amount of Pt used in their catalysts, but they need to maintain high activity, durability, and stability. NWs are an opportunity to meet these targets because they provide large surface areas and many active sites for the catalytic reaction while preventing Ostwald ripening, aggregation, and dissolution.[18,19] In addition, they are good conductors and can be used as templates for catalyst development.[20]

NWs can be used as templates by implementing the spontaneous galvanic displacement (SGD) method.[21] This process is thermodynamically favorable and occurs when a more noble metal interacts with a less noble metal. Here, the metal ion

https://doi.org/10.1021/acsomega.1c00792
ACS Omega 2021, 6, 17203−17216

with higher reduction potential will have a propensity to reduce at the solid metal surface with a lower reduction potential.[22] Exciting results from the NW arrangement for ORR catalysis can be found. A few are ultrafine jagged Pt-NWs with impressive activity in acidic medium with 13.6 A/mg_{Pt} at 0.90 V versus reversible hydrogen electrode (RHE).[23] Alia *et al.* studied the PtNi-NW catalyst in acid medium resulting in 3- and 10-fold enhancement in specific and mass activity, respectively, compared with the traditional Pt nanoparticle catalyst,[24,25] and Shao *et al.* reported the different syntheses of platinum group metal (PGM) NWs.[20]

In this work, we synthesized Ni-NWs and modified them with Pt by SGD to obtain PtNi-NWs. The morphology, surface, and crystallographic characterizations were studied. The specific and mass activities were evaluated with ORR polarization curves. The durability experiments were done to test the performance of the catalysts in alkaline medium. Additionally, *in situ* X-ray absorption spectroscopy (XAS) electrochemical studies were executed to evaluate the geometric and electronic structure of the catalyst while undergoing the ORR at a fixed electrochemical potential in 0.1 M KOH.

2. RESULTS AND DISCUSSION

2.1. Transmission Electron Microscopy. High-resolution TEM was used to examine the morphology of Ni and PtNi catalysts. The Ni particles obtained after solvothermal synthesis exhibited an NW structure as shown in Figure 1a,b, with an average diameter of 96 ± 28 nm and an average length of 590 ± 212 nm (Figure S1). These images exhibited ramifications of the Ni-NWs with different observed sizes. The synthesis of choice required the use of ethylene glycol (EG) because it acts as a reducing agent, preventing particle agglomeration, thus acting as a stabilizing agent. The use of EG led to the formation of these ramifications while preventing the agglomeration of the Ni particles resulting in the wire morphology. A high-resolution TEM image of the Ni-NWs is shown in Figure 1c,d; the green, yellow, and brown rings in the fast Fourier transform (FFT) spots of the high-resolution TEM image of the Ni-NWs correspond to the lattice spacings 2.4, 2.1, and 1.5 Å, respectively. These spots are related to the planes 111, 002, and 022 of the crystalline structure of Ni oxide (NiO) (98-000-9861). The yellow and red rings correspond to the lattice spacings 2.1 and 1.8 Å, respectively, related to the 111 and 002 planes of metallic Ni (Ni°) of the Ni-NWs (see also Figure S2). Ni° and NiO are present in the structure of the Ni-NWs according to this analysis and in another spot of the Ni-NWs (see Figure S3). This indicates that a portion of the Ni-NWs was reduced, eventually serving as a template to form the PtNi-NWs. The Pt deposition on the Ni-NWs was done using the SGD. TEM on the PtNi-NWs provided evidence of their formation through the SGD (Figure 1e,f). These images showed a difference in contrast between the brighter inner cores and darker outer layers of the NWs, suggesting that the cores comprise Ni (lower mass), while the shell layers consist of Pt (higher mass). This structure is also confirmed with the EDS spectrum (Figure 2a) and the EDS mapping (Figure 2c−e). In the spectrum, we see the presence of Pt and Ni, and when we overlay the EDS map of Ni and Pt, Ni is on the inside of the NW and Pt on the outside.

According to the EDS data, the atomic composition of the PtNi-NW catalyst was 3:1 Pt/Ni (Table S2). Furthermore, ICP-optical emission spectroscopy was used to confirm the Pt/Ni ratio and weight concentration (Table S3.). ICP showed a relationship of 1:2 Pt/Ni, and the wt % concentrations were 60.9 ± 0.9 and 39.1 ± 1, for Pt and Ni, respectively. These ICP values were used for all the experimental procedures.

2.2. X-ray Powder Diffraction. X-ray powder diffraction was used to corroborate the presence of the reduced crystalline patterns of Ni from the Ni-NW synthesis and the presence of Pt and Ni after the galvanic displacement. For the Ni-NWs, diffraction peaks of 2θ values at 44.5, 51.8, 76.4, 92.9, and 98.5° were found (Figure 3a). These reflections correspond to the

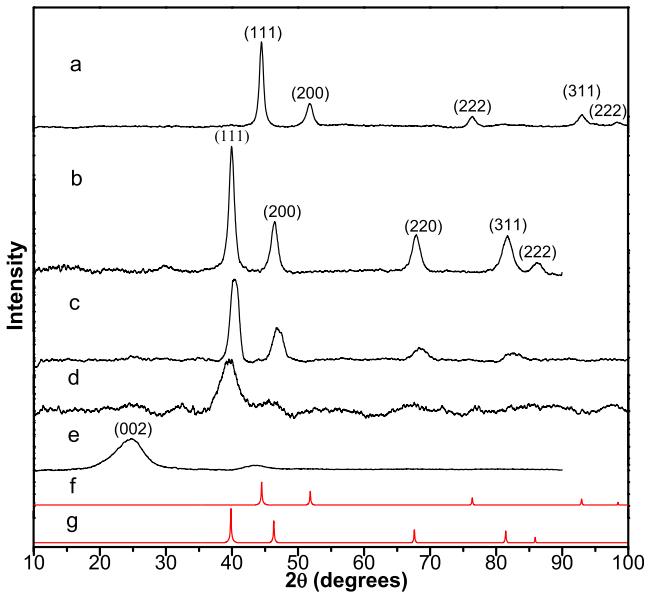

Figure 3. XRD patterns of Ni-NWs (a), PtNi-NWs (b), and PtNi-NWs/Carbon Vulcan XC-72R (V) (c), together with commercial Pt/V (d) and commercial V (e). Standard peak of Ni from 64989 Inorganic Crystal Structure Database (f) and Pt from 0018004 American Mineralogist Crystal Structure Database for comparison (g).

face-centered cubic (fcc) lattice structure assigned to the (111), (200), (220), (311), and (222) Miller indexes of Ni, respectively.[26] For the PtNi-NWs, the Pt diffraction patterns are assigned to the fcc lattice of Pt. Bragg's reflection signals of 2θ value (Figure 3b) at 39.9° (111), 46.5° (200), 67.9° (220), 81.8° (311), and 86.4° (222) attributed to fcc Pt.[27−30] This may be due to an alloy formation between Pt and Ni.[28] Because the reduction of Pt on Ni was carried out in the aqueous solution at 90 °C, the Ni species present in the PtNi-NWs may be oxidized or in an amorphous nature. This result will be reflected in the presence of just the crystalline structure of Pt in the PtNi-NW pattern.[31]

2.3. X-ray Photoelectron Spectroscopy. XPS was done to examine the Pt and Ni oxidation states at the surface of the material. Figure 4a reveals the survey data obtained for both Ni-NW and PtNi-NW samples. Figure 4b shows a deconvoluted spectrum of Ni-NWs using the Ni 2p region. The spectrum showed speciation of Ni atoms in different oxidation states as oxide and hydroxide species. The atomic percentage (at. %) was calculated according to the deconvoluted relative peak areas (Table 1), resulting in at. % of 23.0, 30.4, and 46.6% for NiOOH, $Ni(OH)_2$, and NiO, respectively.[32]

2.4. *Ex Situ* XAS. According to the high-resolution TEM, FFT, and the XRD patterns on the Ni-NWs there is Ni° (see Figures 1c,d, S2, S3, and 3a), allowing the SGD with Pt. However, in the XPS spectrums, the Ni° peak is missing on the

https://doi.org/10.1021/acsomega.1c00792
ACS Omega 2021, 6, 17203−17216

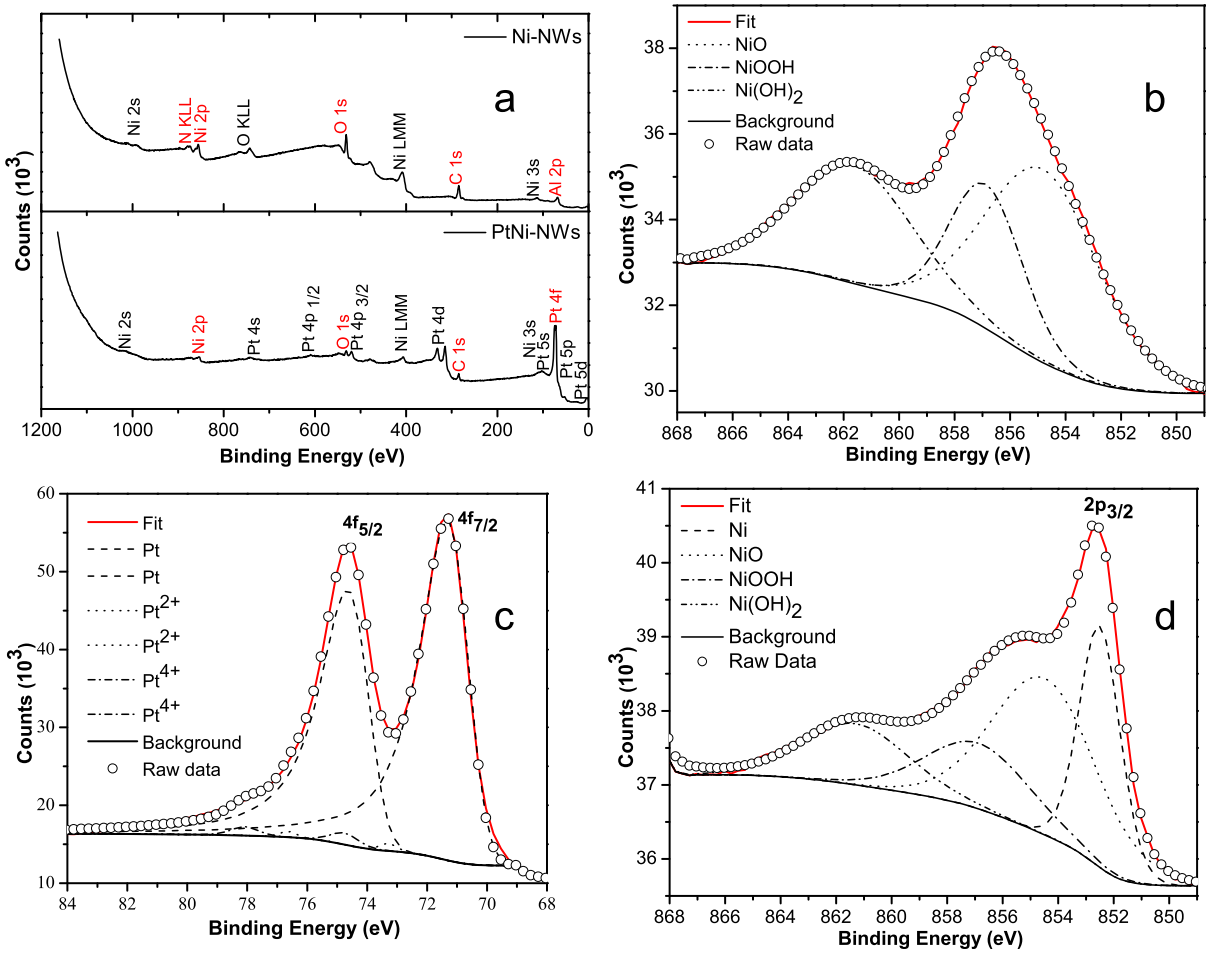

Figure 4. Peak deconvolutions of the Pt 4f and Ni 2p bind energy region. (a) Survey data of Ni-NWs and PtNi-NWs. (b) Peak deconvolutions of Ni-NWs. Peak deconvolutions of Pt (c) and Ni (d) of the PtNi-NW sample.

Table 1. Physicochemical Properties of Pt $4f_{7/2}$ and Ni $2p_{3/2}$ Binding Energy Regions

sample	PtNi-NWs							Ni-NWs		
chemical composition	Pt	Pt^{2+}	Pt^{4+}	Ni	NiO	NiOOH	$Ni(OH)_2$	NiO	NiOOH	$Ni(OH)_2$
position (BE) eV	70.8	73.3	74.8	852.5	854.5	856.9	861.3	854.8	856.9	861.6
FWHM	1.6	0.6	1.1	1.7	4.5	4.5	4.5	4.7	3.1	5.0
at. %	97.8	0.6	1.6	25.1	41.4	17.4	14.2	46.6	23.0	30.4

Ni-NW sample, suggesting that the sample surface was oxidized, a phenomenon previously observed when Ni is exposed to air at room temperature.[33,34] The Ni-NW width is *ca.* 100 nm, and the XPS signal may originate from less than *ca.* 5 nm of the surface. Figure 4d shows the XPS spectrum of the Ni 2p binding energy region of PtNi-NWs. The spectrum was deconvoluted into four different peak regions. In this sample, Ni° is found at 852.51 eV, and other oxide and hydroxide species are attributed to the other peaks. In agreement with TEM data, the SGD was successfully observed using EDS mapping, corroborating that Ni is inside the PtNi-NWs and Pt is on the outside of the NW (Figure 2). The atomic percentages (at. %) were also calculated according to the deconvoluted relative peak areas (see Table 1), resulting in 14.2, 17.4, 25.1, and 41.4% for $Ni(OH)_2$, NiOOH, Ni°, and NiO, respectively. The Pt 4f binding energy region was deconvoluted and three peaks were obtained, as shown in Figure 4c. Predominantly, Pt° is observed with an at. % of 97.8% at 70.83 eV. Other Pt oxide species were assigned at 73.29 eV (Pt^{2+}) and 74.76 eV (Pt^{4+}). Because Pt was expected to be reduced during the SGD procedure, these XPS results confirm this assumption. It is also essential to consider that Pt may be donating electronic density to Ni because at first, in the Ni-NW sample, Ni° was not present, and after the SGD (PtNi-NWs), Ni° was found. To further corroborate this premise, *ex situ* XAS analysis was used.

The XAS experiments were done first to compare the chemical properties of the ORR catalyst with previous *ex situ* characterizations. Mainly, the *ex situ* XAS data (see Figure 5) can be related to the XPS results. Previously, the XPS results raise the following question regarding why Ni° is missing in the linear combination analysis of the 2p peak: (i) only the Ni surface of the Ni-NW sample was oxidized in the air or chemically (see Figure 4b) or (ii) Ni obtained electron density from Pt deposited on the Ni-NW surfaces by the SGD, resulting in Ni° in the Ni XPS from the PtNi-NW sample (see Figure 4d). The *ex situ* XANES data goes in accordance with the statement that Pt is donating electrons to Ni. Figure 5a shows that the order of white line peak intensity in Ni K edge spectra is PtNi-NWs/V > PtNi-

https://doi.org/10.1021/acsomega.1c00792
ACS Omega 2021, 6, 17203−17216

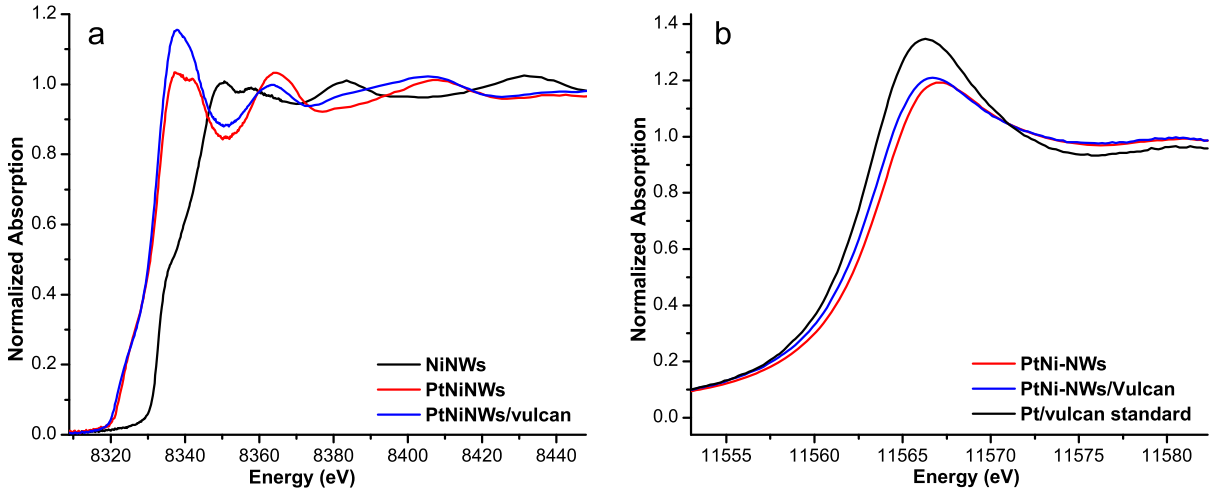

Figure 5. *Ex situ* XANES energy region spectra of (a) Ni K and (b) Pt L_3 edges of PtNi-NWs (red line) and PtNi-NWs/V (blue line). XANES of the (a) Ni-NWs (black line) and (b) Pt/Vulcan standard (black line) for comparison.

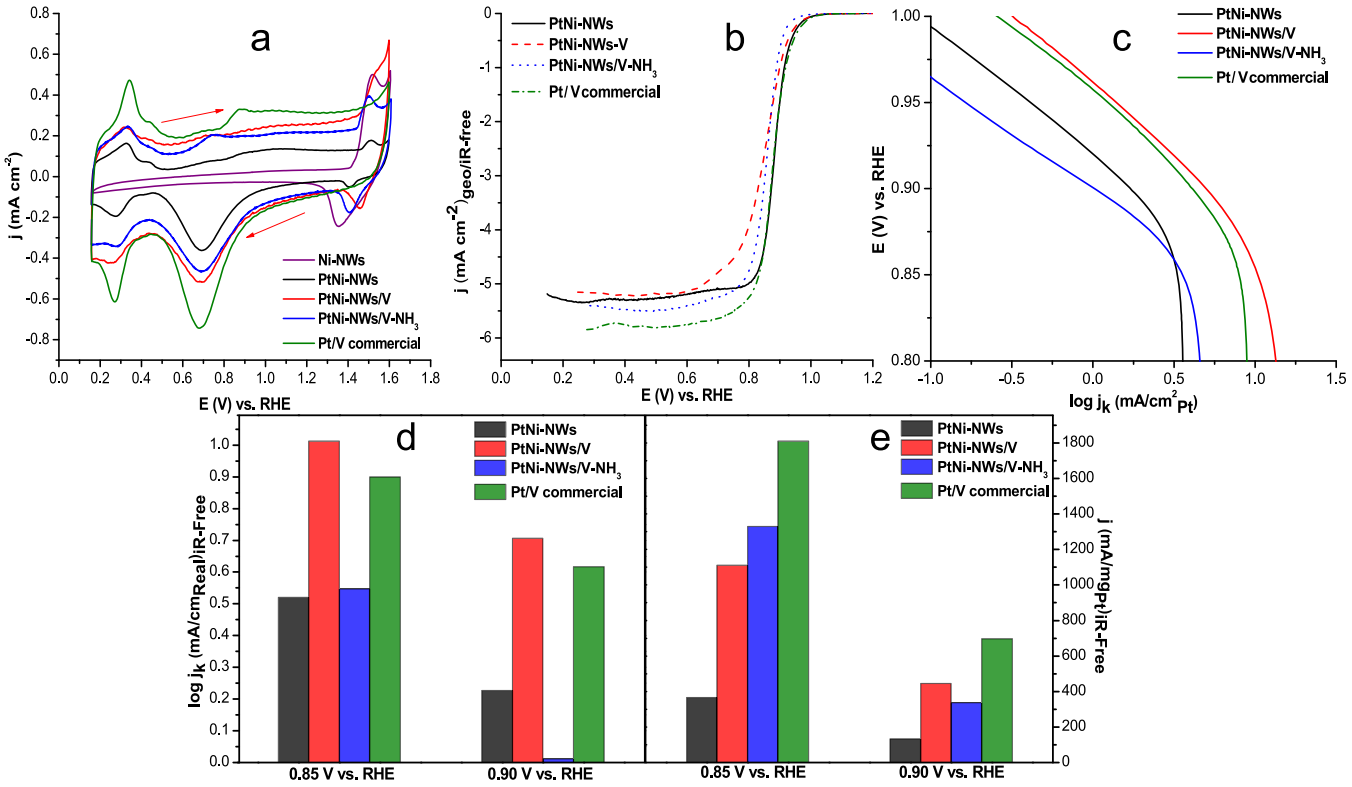

Figure 6. (a) Cyclic voltammograms of Ni-NWs, PtNi-NWs, PtNi-NWs/V, PtNi-NWs/V−NH_3, and commercial Pt/V at 50 mV/s (b) ORR polarization curves of PtNi-NWs, PtNi-NWs/V, PtNi-NWs/V−NH_3, and commercial Pt/Vulcan at a sweep rate of 10 mV/s and a rotation rate of 1600 rpm. Both experiments were carried out in 0.1 M KOH at (25.0 ± 0.1). (c) Tafel plots for ORR curves (b), (d) specific activities for the catalyst tested, and (e) mass activities for the catalysts tested.

NWs > Ni-NWs. In the spectra, a shift toward lower energies for the PtNi-NW/V and PtNi-NW samples, when compared to the Ni-NWs, is observed. As shown in the Pt L_3 edge spectra in Figure 5b, the order of the white line peak intensity is commercial Pt/V > PtNi-NWs/V > PtNi-NWs, and in the PtNi-NW and PtNi-NW/V samples, Pt has a lower white line intensity than the commercial Pt/V catalyst. Our following approach focused on evaluating if these trends, in both Pt and Ni edges, remain the same undergoing the electrochemical *in situ* experiments in alkaline electrolytes.

2.5. ORR Catalytic Activity. As shown in Figure S4a, a mass loading study was considered to follow the optimal loading ratio of the catalysts. The optimal loading of Pt resulted in 12 $\mu g_{Pt}/cm^2$ with an $E_{1/2}$ = 0.87 V. The mass activities for the different mass loadings at 0.85 and 0.90 V are presented in Figure S4b as well as Tables S5 and S6. The PtNi-NWs/V with 12 $\mu g_{Pt}/cm^2$ resulted in 446 mA/mg_{Pt} at 0.90 V, complying with the DOE 2020 targets for the membrane electrode assembly (MEA) of PGM catalysts.[35] For the sample with 0.060 mg_{Pt}/cm^2 loading, 98 mA/mg_{Pt} was obtained at 0.90 $V_{iR\text{-free}}$. This is a significant difference in terms of activity. Thus, the mass loading of 12 $\mu g_{Pt}/$

https://doi.org/10.1021/acsomega.1c00792
ACS Omega 2021, 6, 17203−17216

Table 2. Summary of Oxygen Reduction Properties of All Catalysts in Alkaline Medium

catalyst	mass loading ($\mu g/cm^2$)$_{geo}$	$E_{1/2}$ (V) *vs* RHE	specific activity (mA/cm^2)$_{Pt}$		mass activity (mA/mg$_{Pt}$)	
			0.90 V	0.85 V	0.90 V	0.85 V
PtNi-NWs	100	0.89 V	0.23	0.52	133	365
PtNi-NWs/V	100	0.87 V	0.71	1.01	446	1110
PtNi-NWs/V−NH_3	100	0.86 V	0.01	0.55	337	1329
commercial Pt/V	60	0.88 V	0.62	0.90	696	1810

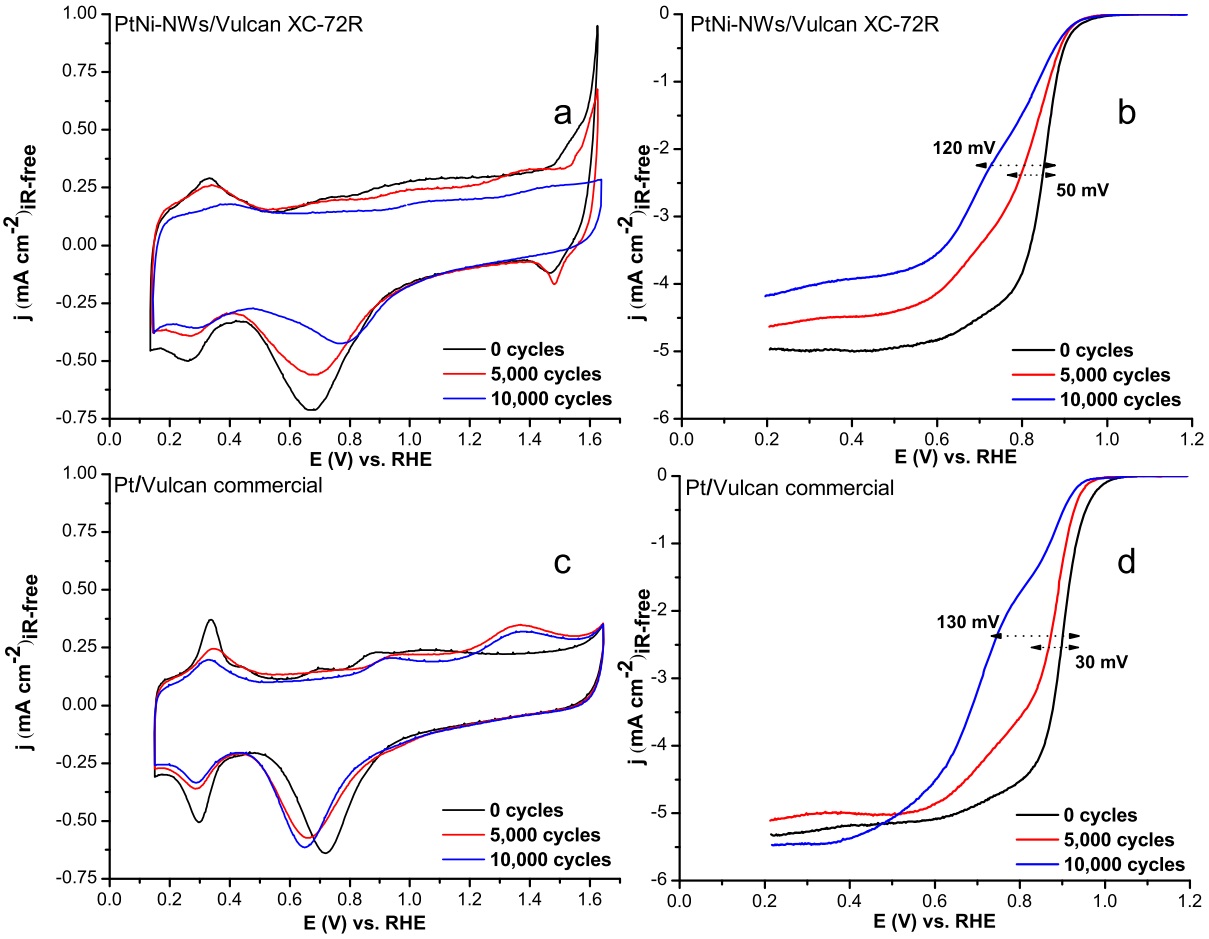

Figure 7. Cyclic voltammograms (a,c) and O_2 polarization curves (b,d) of PtNi-NWs/V before and after 5000 and 10,000 cycles in 0.1 M KOH at 100 mV/s with the controlled temperature at 25.0 ± 0.1 °C.

cm^2 was used for the remaining experiments. If we compare this mass loading to the DOE 2020 target (125 μg_{PGM}/cm$^2{}_{electrode\ area}$) for the MEA, our loadings are lower and are still able to achieve the mass activity suggested by their standards, suggesting a promising activity for our ORR electrocatalysts.

To confirm that our catalyst followed a four-electron pathway, Koutecký−Levich plots (see Figure S5) were used on the PtNi-NW and PtNi-NW/V catalysts, which exhibited 3.8 ± 0.1 and 3.83 ± 0.09 electrons transferred in the ORR, respectively. These results demonstrate that the reaction proceeds through the four-electron pathway with or without the presence of Vulcan XC-72R.

Figure 6a shows cyclic voltammograms of the PtNi-NWs, and PtNi-NW/V cyclic voltammograms show similar peaks and potential regions. The main difference was an increment in the double layer current observed for the PtNi-NWs/V, which could be caused by an increase in the surface area of the catalyst due to carbon. These cyclic voltammograms also justify that both Pt and Ni are electrochemically active on the surface because the signal of the electrochemical behavior of the Ni redox process[36,37] [$Ni(OH)_2 \rightarrow NiOOH + H^+ + e^-$] is observed for oxidation at 1.45 V and reduction at 1.40 V (see Figure S6), and the shape of the voltammogram in the more negative potentials represents the cyclic voltammogram patterns of Pt for hydrogen adsorption−desorption processes (see Figure S7).

The cyclic voltammograms from Pt-containing catalysts (see Figure 6a) were normalized by the Pt electrochemical surface areas calculated from the hydrogen desorption (H_{UPD}) region.[38] Figure 6b shows ORR polarization curves of PtNi catalysts and commercial Pt/V. The limiting diffusion current from each ORR curve shown in Figure 6b was used to obtain the Tafel plot shown in Figure 6c using the following equation

$$j_k = \frac{j_{dif} \times j}{j_{dif} - j} \times \left(\frac{1}{r_f \times A_{geo}}\right) \quad (1)$$

https://doi.org/10.1021/acsomega.1c00792
ACS Omega 2021, 6, 17203−17216

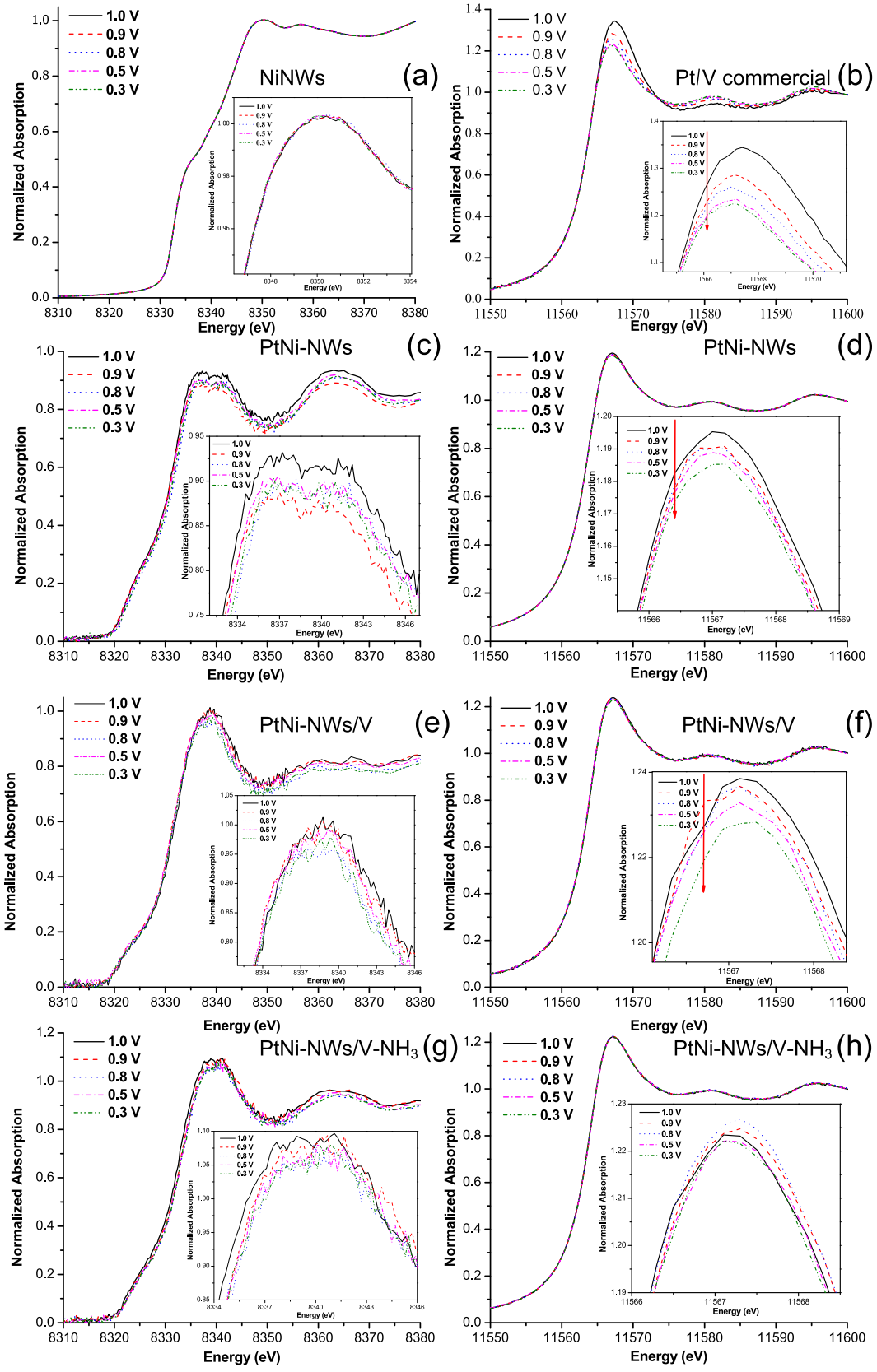

Figure 8. *In situ* XANES region of (a,c,e,g) the Ni K energy edge and (b,d,f,h) Pt L_3 energy edge with different electrochemical applied potentials: (a,b) Ni-NWs and commercial Pt/V, respectively, (c,d) PtNi-NWs, (e,f) PtNi-NWs/V, and (g,h) PtNi-NWs/V−NH_3.

where j_k is the kinetic current density, j_{dif} is the diffusion-limited current density, j is the experimental current density normalized by the rotating disk electrode (RDE) geometric area (A_{geo}) (0.1963 cm^2), and r_f is the roughness factor (=platinum surface area/geometric area).[39]

https://doi.org/10.1021/acsomega.1c00792
ACS Omega 2021, 6, 17203−17216

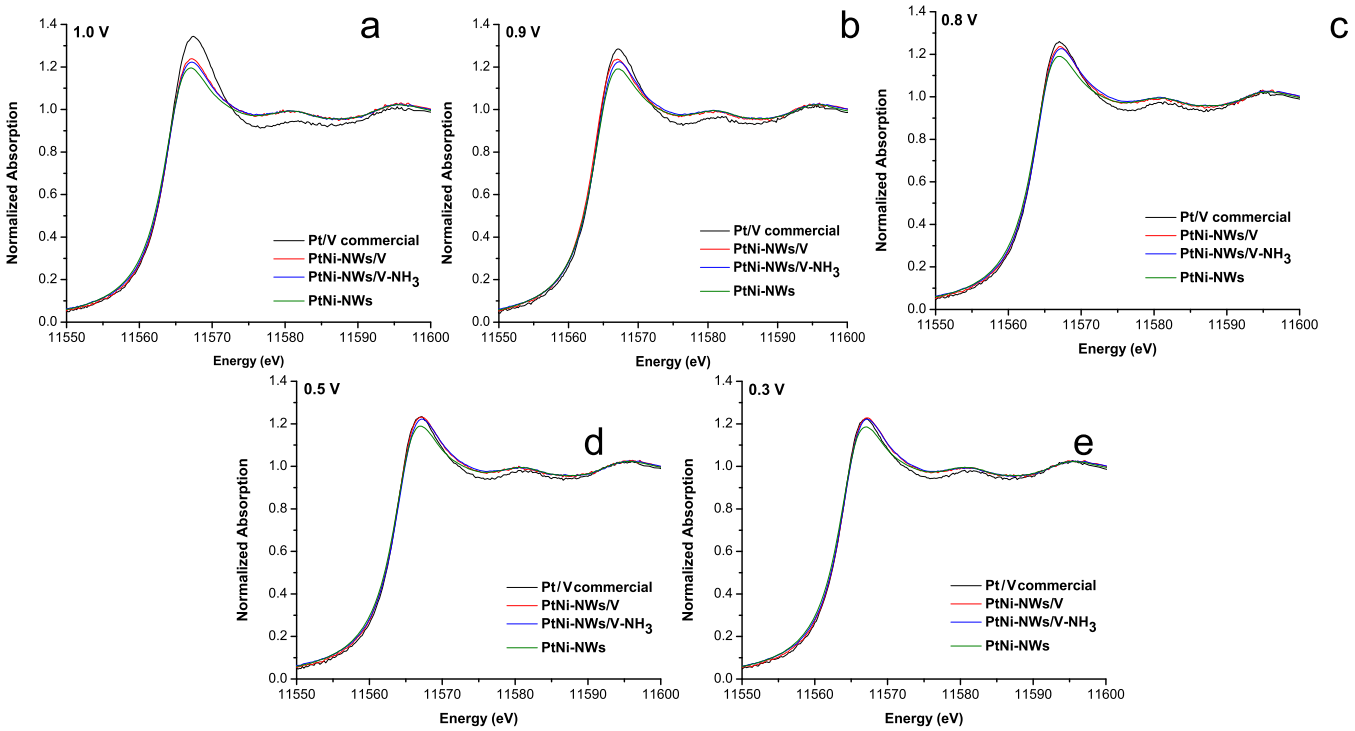

Figure 9. *In situ* XANES of PtNi catalysts at the Pt L_3 energy edge while electrochemical potentials were applied to the *in situ* cell setup: (a) 1.0, (b) 0.9, (c) 0.8, (d) 0.5, and (e) 0.3 V *vs* RHE.

The metal loadings of each catalyst were adjusted by considering their mass. The Pt loadings were always 12 ug_{Pt}/cm^2 normalized to have 0.0024 mg_{Pt} on the glassy carbon (GC) RDE electrode with a geometric area of 0.1963 cm^2 in each experiment for the PtNi-NWs/V (with and without NH_3) and commercial Pt/V catalysts. For the PtNi-NWs, the Pt loading was 0.0118 mg_{Pt}, and for the Ni-NWs, the Ni loading was 0.090 mg_{Ni}. However, when comparing the linear sweep voltammetry (LSV) experiment, shown in Figure 6b, the PtNi-NW, commercial Pt/V, PtNi-NW/V, and PtNi-NW/V−NH_3 catalysts showed $E_{1/2}$ at 0.89, 0.88, 0.87, and 0.86 V, respectively. Our catalysts have closer ORR current densities to the commercial Pt/V catalyst and a higher $E_{1/2}$ value.

The specific activity, mA/cm^2, values at 0.90 and 0.85 V were estimated by extrapolating the Tafel plot. PtNi-NW/V was the most active catalyst with logarithmic values of 0.707 and 1.01 mA/cm^2_{real} at 0.90 and 0.85 V, respectively. Nevertheless, if the mass activity results are compared, commercial Pt/V is more active, showing values of 696 and 1810 mA/mg_{Pt} at 0.90 and 0.85 V, respectively, compared with the PtNi-NWs/V with 446 and 1110 mA/mg_{Pt} (Table 2). It seems that in the PtNi-NW/V catalyst, Pt is not entirely exposed to the surface. This could be due to the large Pt layer on the NW that was observed in the TEM studies (*ca.* 10 nm) (see Figure 1f). When compared with the commercial catalyst that has smaller particle sizes, this translates to better Pt surface interaction in the ORR process for our PtNi-NW samples. An approach to reduce the Pt layer of the PtNi-NW catalyst to a smaller thickness could enhance its mass activity and half-wave potential.

2.6. Durability Experiments. The performance of the PtNi-NWs was evaluated with a durability test where the potential was cycled between 0.60 and 1.00 V (see Figure S8.). Figure 7 shows the cyclic voltammograms and O_2 polarization curves of both PtNi-NWs/V and commercial Pt/V at different steps of the durability test. The cyclic voltammogram of the PtNi-NWs/V before performing the durability test shows the presence of Ni; however, after 5000 cycles, the region where the NiO cathodic and anodic peaks (*ca.* 1.55 and 1.50 V, respectively) are seen exhibits a decrease in current. This may be associated with having less Ni in the middle of the cyclic voltammogram. Similarly, the performance of the catalysts decreases in their $E_{1/2}$ (by 50 mV) after 5000 cycle testing, as shown in Figure 7b. After 10,000 cycles, the NiO cathodic and anodic peaks (*ca.* 1.55 and 1.50 V, respectively) are not seen. Similarly, the performance of the catalysts is lost, showing a decrease in their $E_{1/2}$ (by 120 mV) after 10,000 cycles.

This could happen due to the dissolution of PtNi in KOH.[40,41] This is observed in the cyclic voltammograms of the lab-made catalysts, specifically in the double layer region where it decreases in current as more cycles are performed and the NiO region. When the cyclic voltammogram was recorded before the final LSV (10,000 cycles), the peaks associated with NiO were missing (Figure 7a). Because the cyclic voltammogram shows the process happening at the surface of the working electrode, we could expect that with the absence of NiO peaks and a decrease of current in the double layer region,[42] PtNi is dissolving in KOH; alternatively, a portion of the catalyst layer was lost in solution after 10,000 cycles due to a poor ink composition.[43] The absence of the PtNi material in the working electrode (WE) surface will be translated to lower performance in the LSV experiments, as evidenced in Figure 7b. When our lab-made catalyst was compared with the commercial Pt/V catalyst, the cyclic voltammogram also changes along with the experiment and the O_2 polarization curves. The performance of the commercial Pt/V catalyst is lost through the cycles (time) by 130 mV (Figure 7d). The loss in activity is consistent with both materials suggesting that our catalyst behaves similarly to a commercial FC grade Pt/V catalyst in alkaline medium.

https://doi.org/10.1021/acsomega.1c00792
ACS Omega 2021, 6, 17203−17216

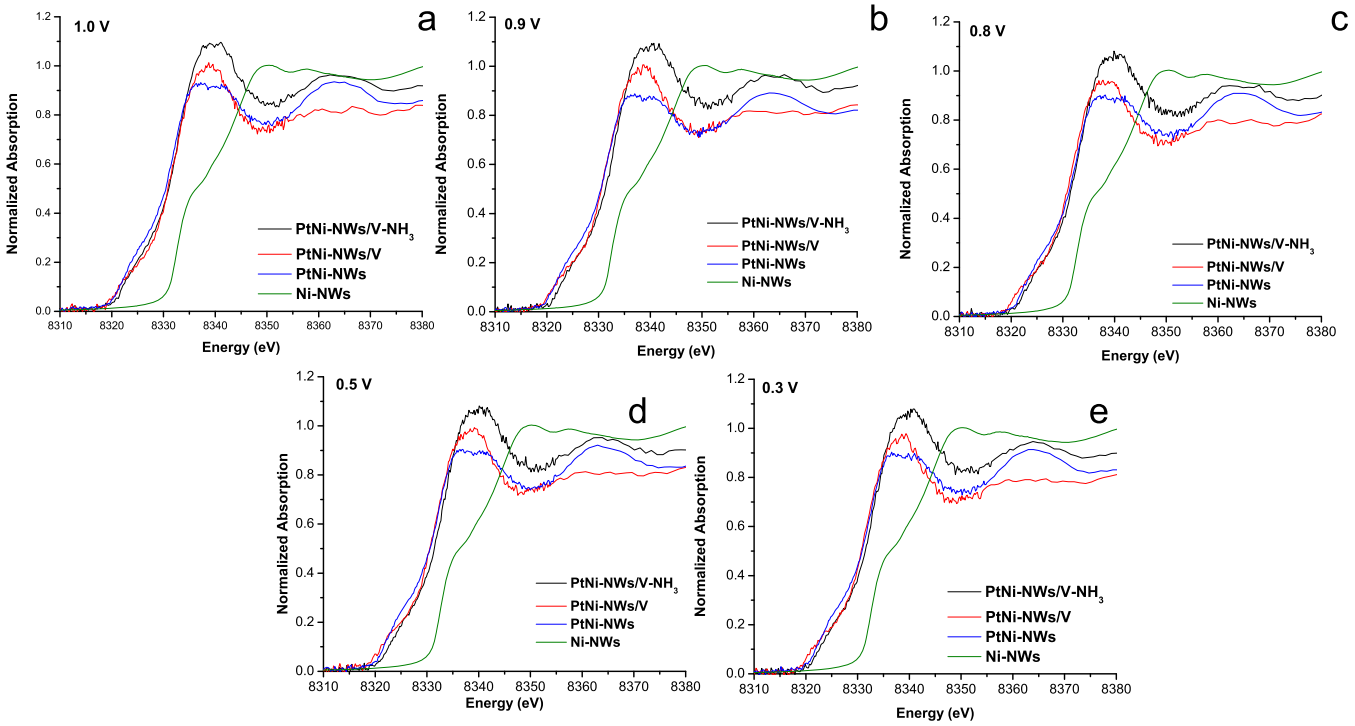

Figure 10. *In situ* XANES of PtNi catalysts at the Ni K edge while electrochemical potentials were applied to the *in situ* cell setup: (a) 1.0, (b) 0.9, (c) 0.8, (d) 0.5, and (e) 0.3 V *vs* RHE.

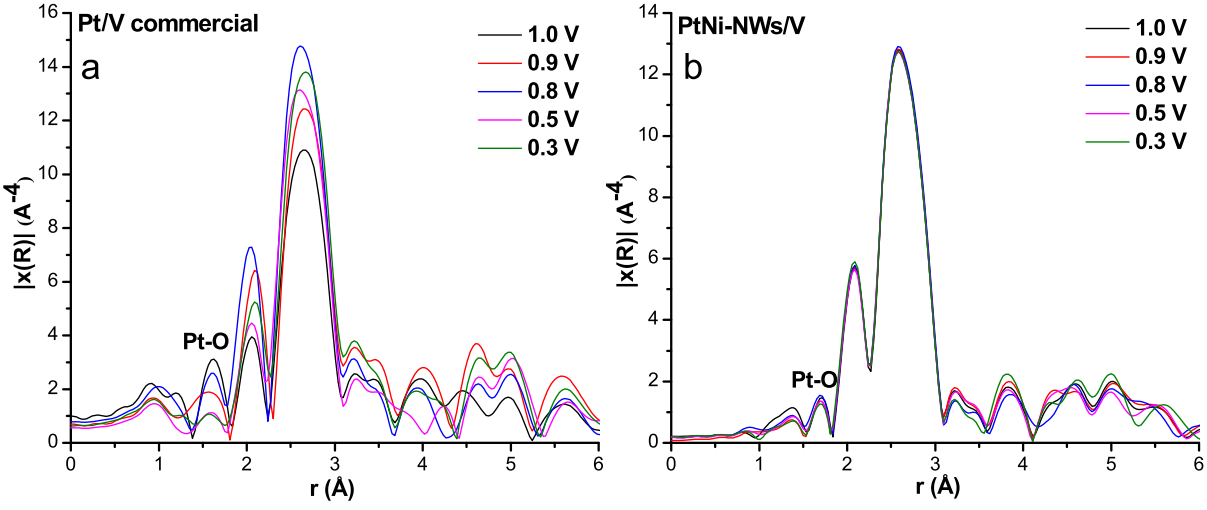

Figure 11. Fourier transform (FT) of the *in situ* electrochemical XAS extended X-ray absorption fine structure (EXAFS) region of (a) commercial Pt/V and (b) PtNi-NWs/V at applied potentials of 1.0, 0.9, 0.8, 0.5, and 0.3 V *vs* RHE in 0.1 M KOH.

2.7. *In Situ* XAS. To understand the local environment of the PtNi catalyst, we performed *in situ* XAS under electrochemical controls. Figure 8 shows XANES spectra of the Ni K edge and Pt L_3 edge of the Ni-NW, commercial Pt/V, PtNi-NW, PtNi-NW/V, and PtNi-NW/V−NH_3 catalysts, where different potentials (from 1.0 to 0.3 V) were applied using chronoamperometry (see Figure S9). Changes in the applied potentials to the electrochemical system were closely monitored with their respective spectroscopic response in the form of changes in the white line intensity of the Ni K and Pt L_3 edges. A trend was observed where at positive applied potentials, the white line intensity peak of the Pt L_3 edge increased. In contrast, when more negative potentials were applied (associated with absorption of oxygenated species in the Pt 5d band),[44] the white line intensity decreased for all the examined catalysts (see Figure 8b,d,f,h). The commercial Pt/V data presented in Figure 8b showed changes in the white line intensity similar to those of our PtNi-NW catalysts (Figure 8d,f). However, for the PtNi-NWs/V−NH_3 (Figure 8h), the changes were smaller in the white line intensity (<2%). This may be due to a less active material as seen in the LSV results (see Figure 6b). These white line changes were also observed when evaluating the Pt L_3 edge catalyst *in situ* XANES response simultaneously at each applied ORR potential (see Figure 9). As the potential was more negative, the Pt L_3 white line intensity peak of all the catalysts decreased; this is associated with less affinities to OH^- absorbed species in the Pt layer previously seen for the Pt catalyst in acidic medium.[45]

https://doi.org/10.1021/acsomega.1c00792
ACS Omega 2021, 6, 17203−17216

Table 3. Structural Parameters Derived from the Pt L_3 Edge XANES and EXAFS Studying the PtNi-NWs/V[a]

sample	edge	near neighbor species	N	R (Å)	σ (Å^2)	E_0 (eV)
Pt foil	Pt L_3	Pt	12	2.764 ± 0.003	0.0055 ± 0.0002	8.0 ± 0.5
Pt 1.0 V_air	Pt L_3	Ni	6	2.66 ± 0.03	0.006 ± 0.003	7.8 ± 0.3
		Pt	8.05	2.74 ± 0.03	0.0054 ± 0.0003	
Pt 0.9 V_air	Pt L_3	Ni	6	2.66 ± 0.03	0.005 ± 0.003	7.7 ± 0.7
		Pt	8.15	2.74 ± 0.03	0.0054 ± 0.0003	
Pt 0.8 V_air	Pt L_3	Ni	6	2.65 ± 0.03	0.003 ± 0.003	7.5 ± 0.4
		Pt	8.5	2.75 ± 0.03	0.0054 ± 0.0003	
Pt 0.5 V_air	Pt L_3	Ni	6	2.66 ± 0.03	0.005 ± 0.003	7.4 ± 0.4
		Pt	8.35	2.74 ± 0.03	0.0055 ± 0.0003	
Pt 0.3 V_air	Pt L_3	Ni	6	2.66 ± 0.03	0.006 ± 0.004	7.0 ± 0.4
		Pt	8.2	2.75 ± 0.03	0.0054 ± 0.0003	

[a]± = uncertainty.

This could be related to changes in oxidation states associated with Pt (Pt L_3 edge). These results are expected because negative potentials are associated with the reduction of PtO. If the peak of the Pt L_3 edge white line decreases in the same trend as the negative potentials are applied, the system responds to the applied potential. Therefore, Pt actively participates in the O_2 reduction process because the air was purged in the solution as potentials were changed. This experiment was also done using the Ni K edge (see Figure 8a,c,e,g). However, no trend was found between the electrochemical potentials and the white line peak for neither of the catalysts. Similarly, when evaluating the catalyst *in situ* response simultaneously at each potential, there are no changes in the white line peak intensity for the PtNi catalysts in the Ni K edge (see Figure 10). This reveals that according to the used method, the electronic properties of Ni are not influenced as the potentials are applied while air is purged in the *in situ* cell alkaline medium.

The ORR active element in our catalyst is Pt. However, when Pt is alloyed to first-row transition metals (M = Co, Fe, or Ni), the Pt/M 5d vacancies are increased compared with having Pt or M alone because M has additional holes in its 5d shell compared with Pt.[46] This effect reduces the interactions of Pt with oxygenated species (OH^-), providing more actives sites for the interaction of Pt with O_2.[47]

In situ EXAFS region FTs of commercial Pt/V and PtNi-NWs/V are presented in Figure 11. The FT EXAFS of commercial Pt/V has evident changes in the Pt/O distance (*ca.* 1.6 Å) as potentials were applied to the electrochemical system. The distances read off the FT may have a phase shift, so an apparent value of 1.6 A may be a distance of 0.2−0.5 A longer. However, the PtNi-NW catalyst showed minimal changes in the Pt/O region. This could be related to no Pt/O interaction, suggesting an alloy interaction of Pt/Ni with O_2.[48] The interaction of Pt/O in PtNi-NWs/V is weaker in all applied potentials with applied 1.0, 0.9, and 0.8 V to commercial Pt/V. This can be associated with Pt oxidation/dissolution inhibition from the PtNi-NW catalyst.[49]

Additionally, when we evaluated the Pt/Pt distances at the Pt L_3 edge, there were no changes with the applied potentials (see Table 3). However, when we compare the Pt/Pt distance of the *in situ* samples with the Pt foil *ex situ* samples, the radial distances varied from 2.764 to 2.744 Å (see Table 3). A lower Pt/Pt bond length (Pt/Pt contraction) is associated with better ORR activity,[50] indicating that PtNi-NWs/V can be further enhanced to provide better catalytic performance and response in alkaline medium.

3. CONCLUSIONS

Thermal reduction and SGD methods were used to synthesize Ni-NWs and PtNi-NWs. The ORR performance of PtNi-NWs/V was examined in 0.1 M KOH by cyclic voltammograms and O_2 polarization curves. The Pt mass loading was lower than DOE MEA guidelines (125 $\mu g_{PGM}/cm^2$), and we still complied DOE mass activity targets for 2020 (440 mA/mg_{PGM}) with 446 mA/mg_{Pt} at 0.90 V versus RHE. The use of a temperature-controlled electrochemical cell improved the O_2 polarization curves of our catalyst by ensuring a constant temperature of 25.0 ± 0.1 °C throughout the experiments. The PtNi-NW catalyst exhibited a four e^- pathway with a value of 3.83 ± 0.09 of electrons calculated according to the Koutecký−Levich equation. The specific activity of PtNi-NWs/V was superior to all the catalysts, including commercial Pt/V. Improvements in the mass activities and $E_{1/2}$ potentials suggest a potential for future use of the PtNi-NW catalysts in AEMFCs. However, the Pt layer thickness at the PtNi-NWs needs to be optimized, and the N_2/NH_3 annealing process may enhance the ORR performance as shown in previous publications.[51]

Studies evaluating the relationship of the Pt mass loading and the ORR performance (*e.g.*, durability experiments) should be done to guarantee the durability of the catalyst while using less Pt mass in the cathode electrode. *In situ* electrochemical XAS was used to evaluate the electronic properties of Ni and Pt. The studies showed that the electronic properties of Pt changed when employing electrochemical potentials associated with ORR in alkaline media. As more negative potentials were applied, the Pt L_3 XAS white line decreased, indicating a less oxidized catalytic material as previously seen in acid media, suggesting that *in situ* electronic properties of Pt are similar in alkaline and acid media. The EXAFS data reveal that PtNi is an alloy because the Pt/O peak remained constant as the electrochemical potentials were applied, suggesting that the interaction with O_2 while ORR is with the whole material (PtNi), not just Pt.

4. RESEARCH DESIGN AND METHODS

4.1. Catalyst Synthesis. The synthesis of the Pt/Ni catalyst was divided into two steps: (1) the Ni-NWs were synthesized and (2) modified with H_2PtCl_6 (Sigma-Aldrich)—a Pt precursor—to build the PtNi-NWs. For the synthesis of the Ni-NWs, a similar hydrothermal synthesis procedure was followed from the studies by Krishnadas *et al.*[52] Briefly, 7.5 mL of total solution composed of aqueous solution of 10 mM $NiCl_2$ (Sigma-Aldrich) and EG (Sigma-Aldrich) was heated up

https://doi.org/10.1021/acsomega.1c00792
ACS Omega 2021, 6, 17203−17216

to 120 °C in an oil bath inside a 50.00 mL round flask with a magnetic stirrer. Then, when the temperature in the 50.00 mL round flask reached 120 °C, 0.1 mL of hydrazine hydrate (Sigma-Aldrich) was added slowly five times every 1 min. In the end, a total of 0.5 mL of hydrazine hydrate was added to the solution (it went from a light blue to a black color). This solution was stirred for 10 min and cooled at ambient temperature for 1 h. The solution was separated at 3400 rpm using a centrifuge (Cole Palmer 17250-10). The solid was rinsed using ethanol (Sigma-Aldrich), isopropanol (Sigma-Aldrich), and nanopure water (18.2 MΩ·cm). Then, the catalyst was dried using an oven (Lindberg/Blue MO1450A-1) for 24 h at 60 °C. Finally, the remaining catalyst was ground by hand—with light pressure—using a small quartz mortar to obtain a powder material.

PtNi-NWs were obtained with SGD considering Pt and Ni standard potentials (Table S1.) and following the procedure from the studies by Alia *et al.*[25] In typical synthesis, 80 mg of lab-made Ni-NWs was added to a 250 mL bottom round flask with 160 mL of pure water and heated at 90 °C in an oil bath. A premade aqueous solution of 15 mL of 10 mM H_2PtCl_6 was added to the bottom round flask with the lab-made Ni-NWs in intervals of 15 min. The whole mixture was mixed with a magnetic stirrer and left for 2 h at 90 °C. The remaining solution was taken out (of the oil bath) and left to cool down to ambient temperature. The resulting PtNi-NWs were dried using the same procedure as the previously synthesized Ni-NWs. V and PtNi-NWs were added to a 150 mL beaker with 100 mL of ethanol. Then, the dispersion was sonicated for 1 h and dried following the same procedure described earlier. The remaining catalyst (PtNi-NWs/V) was in a proportion of 80/20 % V and PtNi-NWs. PtNi-NW/V samples were annealed at 250 °C in N_2 stream, followed by NH_3 gas up to 510 °C at a heating rate of 4.8 °C/min.

4.2. Electrochemical Characterization. Cyclic voltammetry was used to certify the presence of metallic Ni in the product of the first synthesis and then the characterization of the PtNi-NWs. The electrochemical setup consisted of a three-electrode temperature-controlled cell. The electrochemical cell was cleaned with aqua regia before the experiments to reduce interferences. This jacketed cell is composed of a GC working electrode, a silver−silver chloride (Ag/AgCl sat. KCl) reference electrode, and a platinum counter electrode using Autolab PGSTAT30 with a RDE setup (Pine Instruments). The GC electrode was physically cleaned before every experiment by polishing the GC surface with alumina micropolish (Buehler) while decreasing the value of granular pore size 1.0, 0.5, and 0.03 μm and pure water, in an eight-shape pattern.

The temperature control cell was set at 25.0 ± 0.1 °C using a Nestlab RTE-221 chiller and left for 10 min with the aqueous solution (0.1 M KOH) while its temperature reached 25.0 °C. Then, electrochemical cleaning was executed between 1.0 and 1.6 V versus RHE at 100, 50, and 20 mV/s in 0.1 M KOH. After the surface of the GC electrode was physically and electrochemically cleaned, an ink dispersion of the catalyst was used to modify the surface of the GC electrode. A stock solution was prepared consisting of a ratio of 2:1:1:0.10 volume of ethanol (99.5% Sigma-Aldrich), pure water, isopropanol (Sigma-Aldrich), and 5 μL of Nafion (5% solution in alcohol, Sigma-Aldrich), respectively. The mass addition of the catalyst was added considering the mass loading relationship (eq S1). The catalyst ink dispersion was sonicated for 30 min, and an aliquot of 5 μL was drop cast on the GC electrode surface. The electrode was left at ambient temperature (25 °C) for 15−20 min until the ink dried. Then, a cyclic voltammogram was obtained at the Ni potential window from 1.0 to 1.7 V versus RHE at a scan rate of 20 mV/s in 0.1 M KOH. Similarly to this procedure, PtNi-NW catalysts were characterized, but ultrahigh pure (UHP) N_2 was purged before, for 15 min, to prevent poisoning of the Pt surface while in solution. For PtNi-NWs, the potential window used was different, from 0.0 to 1.7 V versus RHE.

4.3. RDE Experiments. Before the RDE experiments, the solution (0.1 M KOH) was purged using UHP N_2 for 15 min. Later a potential of 1.2 V versus RHE was applied for 30 s, and the LSV measurements were done using the potential window between 1.2 and 0.0 V versus RHE and at a scan rate of 10 mV/s. This voltammetry was used to lower the capacitive currents. Subsequently, the catalysts were activated by cycling the potentials while the rotator was turned on at 1600 rpm in the potential window between 0.0 and 1.2 V versus RHE at 100 mV/s for 15 min while UHP O_2 was purged. An additional LSV was acquired at the potential window of between 1.2 and 0.0 V versus RHE at 10 mV/s. Nyquist plots were used to obtain the uncompensated resistance of the measurements. All the polarization curves were corrected by *iR* [E (V) = E_{RHE} (V) − i (A)R (Ω)]. The measurements were also normalized by the geometric area of the GC RDE (0.1963 cm^2), and the mass loading of the catalyst was used to calculate the mass activity at 0.90 and 0.85 V versus RHE. LSV measurements, under different revolutions per minute, were subsequently done, and these revolutions were 400, 600, 900, 1200, 1600, and 2000 rpm. The limiting currents of these curves were obtained and used to calculate the number of electrons transferred applying the Koutecký−Levich equation, eqs S2[53] and S3.[54]

The durability experiments were done to test the stability of the catalyst for prolonged periods under reaction conditions (0.1 M KOH). The following sequence was followed: (1) A voltammogram was obtained under the UHP N_2 environment using the PtNi potential window between 0.20 and 1.65 V versus RHE at a scan rate of 50 mV/s. (2) Both N_2 and O_2 LSV measurements were recorded as in (1). (3) 5000 cyclic voltammogram cycles between 0.6 and 1.0 V versus RHE, at a scan rate of 100 mV/s, were recorded. (4) Steps (1), (2), and (3) were repeated. (5) The experiment was finalized by recording a third and final cyclic voltammogram as step (1) and LSV measurements as step (2). It is important to clarify that the Ag/AgCl reference electrode used during these 10,000 voltammetric cycles was different from the one used to perform the cyclic voltammetry and polarization curve experiments, as shown in Figure 7. The 0.1 M KOH solution was also changed after the first 5000 cycles and after the 10,000 cycles to prevent solution contamination and shifts in the electrochemical potentials due to possible Ag/AgCl reference electrode inner solution leaks.

The calibration of the reference electrode was done daily to ensure a fixed potential. A commercial RHE electrode (edaq) was used to compare the potential of the Ag/AgCl sat. KCl electrode in 0.5 M H_2SO_4 solution. All the potentials were converted to RHE using the following equation

$$E^{\circ}(\mathrm{RHE}) = E(\mathrm{Ag/AgCl})\exp + \frac{\mathrm{pH}((\ln(10)RT)}{nF} + E(\mathrm{Ag/AgCl})\mathrm{calculated} \quad (2)$$

considering the $[H_3O^+]$ activity, and 20% Pt/V (BASF *ca.* 3−2 nm) was used as a reference catalyst.

https://doi.org/10.1021/acsomega.1c00792
ACS Omega 2021, 6, 17203−17216

The ORR electrocatalytic activity of the PtNi-NWs was evaluated using the O_2 polarization curves. Initially, without the use of a temperature controller, the data gathered were not reproducible. Therefore, after implementing the temperature-controlled system, the reproducibility of the data was obtained. The use of the temperature-controlled electrochemical system is not widely discussed for the ORR reaction; however, there is an urge for using these systems when using the Koutecký−Levich equation (eqs S2 and S3) because several equation constants are temperature-dependent, as well as the Ag/AgCl electrode potential.

4.4. Transmission Electron Microscopy. The structural morphology of the samples was confirmed with a 200 kV field emission FEI F20 high resolution transmission electron microscope from the facilities at the Cornell Center for Materials Research (CCMR) at Cornell University. The samples were prepared on a lacey carbon film of 300 mesh Cu grid (Electron Microscopy Sciences). The chemical composition of the samples was examined with EDS with the scanning transmission electron microscope mode and using an Oxford instruments X-ray detector.

4.5. X-ray Powder Diffraction. X-ray powder diffraction was utilized to determine the diffraction pattern of the PtNi catalysts. A Rigaku SmartLab X-ray diffractometer working with a Cu K_α radiation (λ = 1.54 Å) was used. The 2θ range was scanned between 5 and 100° at a rate of 0.02° s^{-1}. Smart lab software was used for background correction. Origin software was used to finalize the peak processing with the smoothness of the signals using the Savitzky−Golay filter.

4.6. X-ray Photoelectron Spectroscopy. The surface structure of the catalysts was further analyzed using XPS. A PHI 5600ci spectrometer equipped with a polychromatic magnesium source (1253.6 eV) was used at 45° with a hemispherical electron energy analyzer. The resolution/pass energy was 58.7 eV. The powder samples were deposited using copper tape, and the binding energy spectra of Ni and Pt species were studied using CasaXPS software—for peak deconvolutions and speciation attribution. The spectra were corrected with adventitious carbon C 1s binding energy of 284.80 eV. A Shirley background was used for all the analyses. An asymmetrical line shape consisted of Lorentzian asymmetric α, β, and m (were α and β defined the spread of the tail on any side of the Lorentzian component and m specified the Gaussian width used to convolute the Lorentzian curvature) was implemented to the Pt ($4f_{7/2}$) and the Ni ($2p_{3/2}$) components.[32,55] The remaining components of the samples were analyzed with Gaussian (70%) and Lorentzian (30%) line shapes.

4.7. *Ex situ* XAS. X-ray absorption fine structure measurements of the catalysts were done at beamline 7-BM for quick X-ray absorption (QAS) at the National Synchrotron Light Source II (NSLS-II) at Brookhaven National Laboratory (BNL). The Pt K edge data was collected in fluorescence yield mode using a passivated implanted planar silicon detector. Data proceeding was done using the IFEFFIT package.[56]

4.8. *In Situ* XAS. *In situ* XAS experiments were done at beamline 7-BM for QAS at NSLS-II at BNL and at the PIPOXS beamline at Cornell High Energy Synchrotron Source (CHESS). We first started with the preparation of the electrochemical setup using a similar procedure to the one explained earlier with three electrodes and an electrochemical cell. The electrochemical setup consisted of a Ag/AgCl reference electrode, a platinum counter electrode, and a catalyst modified carbon cloth (190 μm thickness and *ca.* 10 mm × 100 mm the geometric area) working electrode. The carbon cloth electrode was obtained from the Fuel Cell Store (AvCarb MGL 190). The experiments were done with a previously published electrochemical *in situ* cell from the studies by Sasaki *et al.*[57] (see Figure S11). We first sonicated 0.1 M KOH for 1 h minimum to ensure no interferences of bubbles with the XAS measurements.

The carbon cloth electrode was modified by preparing similar catalyst ink solution mentioned earlier. This solution was made with a ratio of 1 mg of the catalyst per 1 mL of stock solution (2:1:1:0.10 volume ratio of ethanol, pure water, isopropanol, and 5 μL of 5% of Nafion in alcohol, respectively). The ink solution was sonicated for 30 min, and 200 μL was drop cast on 1 cm^2 of the carbon cloth paper. The catalyst on the carbon paper was exposed to a heat gun until dry. Before the *in situ* measurements, the incident energy was selected using a cryogenically cooled Si(111) monochromator and calibrated to the first inflection point of Ni (8333.0 eV) and Pt (11,564 eV) metal foils. Harmonic rejection was accomplished by using Rh-coated Si vertical and horizontal focusing mirrors inclined at 4 mrad. The electrochemical *in situ* cell, without solution and just the working electrode, was placed at 45° relative to the incident beam. To test for the proper signal of the selected energy edges, 10 X-ray scans were run for each sample. The data were collected via fluorescence mode by using a four-element Vortex detector.

Subsequently, the *in situ* electrochemical cell was filled with 0.1 M KOH solution, and the remaining electrodes, reference and counter electrodes, were placed in the cell. The electrochemical cell was purged with UHP N_2 for 15 min. Before the XAS measurements, cyclic voltammetry measurements were done between −0.85 and 0.65 V versus Ag/AgCl (sat. KCl) to test the electrochemical catalyst response in the *in situ* cell. This was followed by the XAS analyses *via* chronoamperometric measurements at 1.0, 0.9, 0.8, 0.5, and 0.3 V versus RHE for 500 s at each potential. The XAS measurements were recorded simultaneously while performing the electrochemical measurements. The same procedure was completed as the air was allowed inside the *in situ* cell with 0.1 M KOH solution, simulating an oxygen reduction under atmospheric conditions.

■ ASSOCIATED CONTENT

Supporting Information

The Supporting Information is available free of charge at https://pubs.acs.org/doi/10.1021/acsomega.1c00792.

> Electrochemical and physical characterization of PtNi-NWs/V, ORR studies, EDS and ICP data, mass loading studies, Koutecký−Levich analysis, RDE experiments, cyclic voltammograms of the durability experiments, chronoamperometric measurements of the *in situ* XAS experiments, protocol to calibrate the Ag/AgCl reference electrode, and electrochemical *in situ* cell setup (PDF)

■ AUTHOR INFORMATION

Corresponding Authors

Joesene Soto-Pérez − *Department of Chemistry, University of Puerto Rico, San Juan 00925-2537, Puerto Rico*; Email: joesene.soto@upr.edu

Carlos R. Cabrera − *Department of Chemistry, University of Puerto Rico, San Juan 00925-2537, Puerto Rico*; orcid.org/0000-0002-3342-8666; Email: carlos.cabrera2@upr.edu

Authors

Luis E. Betancourt − *Chemistry Division, Brookhaven National Laboratory, Upton, New York 11973, United States*

Pedro Trinidad − *Department of Chemistry, University of Puerto Rico, San Juan 00925-2537, Puerto Rico*

Eduardo Larios − *Departamento de Ingeniería Química y Metalurgia, Universidad de Sonora, Hermosillo 83000, Mexico*

Arnulfo Rojas-Pérez − *Department of Chemistry, University of Puerto Rico, San Juan 00925-2537, Puerto Rico;* orcid.org/0000-0002-3804-6309

Gerardo Quintana − *Department of Chemistry, University of Puerto Rico, San Juan 00925-2537, Puerto Rico*

Kotaro Sasaki − *Chemistry Division, Brookhaven National Laboratory, Upton, New York 11973, United States;* orcid.org/0000-0003-2474-8323

Christopher J. Pollock − *Cornell High Energy Synchrotron Source (CHESS), Wilson Laboratory, Cornell University, Ithaca, New York 14853, United Sates;* orcid.org/0000-0001-5736-513X

Louise M. Debefve − *Cornell High Energy Synchrotron Source (CHESS), Wilson Laboratory, Cornell University, Ithaca, New York 14853, United Sates*

Complete contact information is available at: https://pubs.acs.org/10.1021/acsomega.1c00792

Notes

The authors declare no competing financial interest.

■ ACKNOWLEDGMENTS

This work was supported by the National Science Foundation NSF-PREM: Center for Interfacial Electrochemistry of Energy Materials (CiE^{2}M) grant number DMR-1827622. The use of the Cornell Center for Materials Research Shared Facilities, which is supported through the NSF MRSEC grant number DMR-1719875, is greatly appreciated. This research used resources of the 7-BM QAS beamline of the National Synchrotron Light Source II, a U.S. Department of Energy (DOE) Office of Science User Facility operated for the DOE Office of Science by Brookhaven National Laboratory under contract no. DE-SC0012704. This work is based upon research conducted at the Center for High Energy X-ray Sciences (CHEXS) which is supported by the National Science Foundation under award DMR-1829070.

■ REFERENCES

(1) Banham, D.; Ye, S. Current Status and Future Development of Catalyst Materials and Catalyst Layers for Proton Exchange Membrane Fuel Cells: An Industrial Perspective. *ACS Energy Lett.* **2017**, *2*, 629−638.

(2) Edwards, P. P.; Kuznetsov, V. L.; David, W. I. F.; Brandon, N. P. Hydrogen and Fuel Cells: Towards a Sustainable Energy Future. *Energy Policy* **2008**, *36*, 4356−4362.

(3) Winter, M.; Brodd, R. J. What Are Batteries, Fuel Cells, and Supercapacitors? *Chem. Rev.* **2004**, *104*, 4245−4270.

(4) Ren, X.; Lv, Q.; Liu, L.; Liu, B.; Wang, Y.; Liu, A.; Wu, G. Current Progress of Pt and Pt-Based Electrocatalysts Used for Fuel Cells. *Sustainable Energy Fuels* **2020**, *4*, 15−30.

(5) Demarconnay, L.; Coutanceau, C.; Léger, J.-M. Electroreduction of Dioxygen (ORR) in Alkaline Medium on Ag/C and Pt/C Nanostructured Catalysts—Effect of the Presence of Methanol. *Electrochim. Acta* **2004**, *49*, 4513−4521.

(6) Bu, L.; Zhang, N.; Guo, S.; Zhang, X.; Li, J.; Yao, J.; Wu, T.; Lu, G.; Ma, J.-Y.; Su, D.; Huang, X. Biaxially Strained PtPb/Pt Core/Shell Nanoplate Boosts Oxygen Reduction Catalysis. *Science* **2016**, *354*, 1410−1414.

(7) Wang, D.; Xin, H. L.; Hovden, R.; Wang, H.; Yu, Y.; Muller, D. A.; Disalvo, F. J.; Abruña, H. D. Structurally Ordered Intermetallic Platinum-Cobalt Core-Shell Nanoparticles with Enhanced Activity and Stability as Oxygen Reduction Electrocatalysts. *Nat. Mater.* **2013**, *12*, 81−87.

(8) Shen, L.-L.; Zhang, G.-R.; Miao, S.; Liu, J.; Xu, B.-Q. Core−Shell Nanostructured Au@ Ni m Pt2 Electrocatalysts with Enhanced Activity and Durability for Oxygen Reduction Reaction. *ACS Catal.* **2016**, *6*, 1680−1690.

(9) Ge, X.; Sumboja, A.; Wuu, D.; An, T.; Li, B.; Goh, F. W. T.; Hor, T. S. A.; Zong, Y.; Liu, Z. Oxygen Reduction in Alkaline Media: From Mechanisms to Recent Advances of Catalysts. *ACS Catal.* **2015**, *5*, 4643−4667.

(10) Liang, Y.; Li, Y.; Wang, H.; Zhou, J.; Wang, J.; Regier, T.; Dai, H. Co_3O_4 Nanocrystals on Graphene as a Synergistic Catalyst for Oxygen Reduction Reaction. *Nat. Mater.* **2011**, *10*, 780−786.

(11) Yin, H.; Zhao, S.; Zhao, K.; Muqsit, A.; Tang, H.; Chang, L.; Zhao, H.; Gao, Y.; Tang, Z. Ultrathin Platinum Nanowires Grown on Single-Layered Nickel Hydroxide with High Hydrogen Evolution Activity. *Nat. Commun.* **2015**, *6*, 6430.

(12) Shulda, S.; Weker, J. N.; Ngo, C.; Alia, S. M.; Mauger, S. A.; Neyerlin, K. C.; Pivovar, B. S.; Pylypenko, S. 2D and 3D Characterization of PtNi Nanowire Electrode Composition and Structure. *ACS Appl. Nano Mater.* **2019**, *2*, 525−534.

(13) Kim, M. J.; Cruz, M. A.; Yang, F.; Wiley, B. J. Accelerating Electrochemistry with Metal Nanowires. *Curr. Opin. Electrochem.* **2019**, *16*, 19−27.

(14) Wang, Z.; Cao, X.; Peng, D.; Lu, Y.; Zhang, B.; Huang, K.; Zhang, T.; Wu, J.; Huang, Y. Strained Ultralong Silver Nanowires for Enhanced Electrocatalytic Oxygen Reduction Reaction in Alkaline Medium. *J. Phys. Chem. Lett.* **2021**, *12*, 2029−2035.

(15) Kulkarni, A.; Siahrostami, S.; Patel, A.; Nørskov, J. K. Understanding Catalytic Activity Trends in the Oxygen Reduction Reaction. *Chem. Rev.* **2018**, *118*, 2302−2312.

(16) Darling, R. M.; Meyers, J. P. Kinetic Model of Platinum Dissolution in PEMFCs. *J. Electrochem. Soc.* **2003**, *150*, A1523−A1527.

(17) Stamenkovic, V. R.; Fowler, B.; Mun, B. S.; Wang, G.; Ross, P. N.; Lucas, C. A.; Markovic, N. M. Improved Oxygen Reduction Activity on $Pt_3Ni(111)$ via Increased Surface Site Availability. *Science* **2007**, *315*, 493−497.

(18) Chen, Z.; Waje, M.; Li, W.; Yan, Y. Supportless Pt and PtPd Nanotubes as Electrocatalysts for Oxygen-reduction Reactions. *Angew. Chem., Int. Ed.* **2007**, *46*, 4060−4063.

(19) Mao, J.; Chen, W.; He, D.; Wan, J.; Pei, J.; Dong, J.; Wang, Y.; An, P.; Jin, Z.; Xing, W.; Tang, H.; Zhuang, Z.; Liang, X.; Huang, Y.; Zhou, G.; Wang, L.; Wang, D.; Li, Y. Design of Ultrathin Pt-Mo-Ni Nanowire Catalysts for Ethanol Electrooxidation. *Sci. Adv.* **2017**, *3*, No. e1603068.

(20) Shao, Q.; Lu, K.; Huang, X. Platinum Group Nanowires for Efficient Electrocatalysis. *Small Methods* **2019**, *3*, 1800545.

(21) Chang, Y.-H.; Lin, T.-J.; Wu, Y.-C.; Fan, S.-W.; Lee, Y.-H.; Lai, Y.-R. Surfactant-Assisted Galvanic Synthesis and Growth Characteristics of Copper Nanowires. *Inorg. Chem. Front.* **2019**, *6*, 57−62.

(22) Carraro, C.; Maboudian, R.; Magagnin, L. Metallization and Nanostructuring of Semiconductor Surfaces by Galvanic Displacement Processes. *Surf. Sci. Rep.* **2007**, *62*, 499−525.

(23) Li, M.; Zhao, Z.; Cheng, T.; Fortunelli, A.; Chen, C.-Y.; Yu, R.; Zhang, Q.; Gu, L.; Merinov, B. V.; Lin, Z.; Zhu, E.; Yu, T.; Jia, Q.; Guo, J.; Zhang, L.; Goddard, W. A.; Huang, Y.; Duan, X. Ultrafine Jagged Platinum Nanowires Enable Ultrahigh Mass Activity for the Oxygen Reduction Reaction. *Science* **2016**, *354*, 1414−1419.

(24) Alia, S. M.; Larsen, B. A.; Pylypenko, S.; Cullen, D. A.; Diercks, D. R.; Neyerlin, K. C.; Kocha, S. S.; Pivovar, B. S. Platinum-Coated Nickel Nanowires as Oxygen-Reducing Electrocatalysts. *ACS Catal.* **2014**, *4*, 1114−1119.

(25) Alia, S. M.; Ngo, C.; Shulda, S.; Ha, M.-A.; Dameron, A. A.; Weker, J. N.; Neyerlin, K. C.; Kocha, S. S.; Pylypenko, S.; Pivovar, B. S. Exceptional Oxygen Reduction Reaction Activity and Durability of

Platinum−Nickel Nanowires through Synthesis and Post-Treatment Optimization. *ACS Omega* **2017**, *2*, 1408−1418.
(26) Jia, F. L.; Zhang, L. Z.; Shang, X. Y.; Yang, Y. Non-Aqueous Sol−Gel Approach towards the Controllable Synthesis of Nickel Nanospheres, Nanowires, and Nanoflowers. *Adv. Mater.* **2008**, *20*, 1050−1054.
(27) Park, K.-W.; Choi, J.-H.; Kwon, B.-K.; Lee, S.-A.; Sung, Y.-E.; Ha, H.-Y.; Hong, S.-A.; Kim, H.; Wieckowski, A. Chemical and Electronic Effects of Ni in Pt/Ni and Pt/Ru/Ni Alloy Nanoparticles in Methanol Electrooxidation. *J. Phys. Chem. B* **2002**, *106*, 1869−1877.
(28) Deivaraj, T. C.; Chen, W.; Lee, J. Y. Preparation of PtNi Nanoparticles for the Electrocatalytic Oxidation of Methanol. *J. Mater. Chem.* **2003**, *13*, 2555−2560.
(29) Jiang, Q.; Jiang, L.; Wang, S.; Qi, J.; Sun, G. A Highly Active PtNi/C Electrocatalyst for Methanol Electro-Oxidation in Alkaline Media. *Catal. Commun.* **2010**, *12*, 67−70.
(30) Jia, Q.; Zhao, Z.; Cao, L.; Li, J.; Ghoshal, S.; Davies, V.; Stavitski, E.; Attenkofer, K.; Liu, Z.; Li, M.; Duan, X.; Mukerjee, S.; Mueller, T.; Huang, Y. Roles of Mo Surface Dopants in Enhancing the ORR Performance of Octahedral PtNi Nanoparticles. *Nano Lett.* **2018**, *18*, 798−804.
(31) Fu, X.-Z.; Liang, Y.; Chen, S.-P.; Lin, J.-D.; Liao, D.-W. Pt-Rich Shell Coated Ni Nanoparticles as Catalysts for Methanol Electro-Oxidation in Alkaline Media. *Catal. Commun.* **2009**, *10*, 1893−1897.
(32) Biesinger, M. C.; Payne, B. P.; Lau, L. W. M.; Gerson, A.; Smart, R. S. C. X-Ray Photoelectron Spectroscopic Chemical State Quantification of Mixed Nickel Metal, Oxide and Hydroxide Systems. *Surf. Interface Anal.* **2009**, *41*, 324−332.
(33) Holloway, P. H. Chemisorption and Oxide Formation on Metals: Oxygen-Nickel Reaction. *J. Vac. Sci. Technol.* **1981**, *18*, 653−659.
(34) Lambers, E. S.; Dykstal, C. N.; Seo, J. M.; Rowe, J. E.; Holloway, P. H. Room-Temperature Oxidation of Ni(110) at Low and Atmospheric Oxygen Pressures. *Oxid. Met.* **1996**, *45*, 301−321.
(35) Thompson, S. T.; Wilson, A. R.; Zelenay, P.; Myers, D. J.; More, K. L.; Neyerlin, K. C.; Papageorgopoulos, D. ElectroCat: DOE's Approach to PGM-Free Catalyst and Electrode R&D. *Solid State Ionics* **2018**, *319*, 68−76.
(36) Grdeń, M.; Klimek, K. EQCM Studies on Oxidation of Metallic Nickel Electrode in Basic Solutions. *J. Electroanal. Chem.* **2005**, *581*, 122−131.
(37) Medway, S. L.; Lucas, C. A.; Kowal, A.; Nichols, R. J.; Johnson, D. In Situ Studies of the Oxidation of Nickel Electrodes in Alkaline Solution. *J. Electroanal. Chem.* **2006**, *587*, 172−181.
(38) Garsany, Y.; Baturina, O. A.; Swider-Lyons, K. E.; Kocha, S. S. Experimental Methods for Quantifying the Activity of Platinum Electrocatalysts for the Oxygen Reduction Reaction. *Anal. Chem.* **2010**, *82*, 6321−6328.
(39) Mayrhofer, K. J. J.; Strmcnik, D.; Blizanac, B. B.; Stamenkovic, V.; Arenz, M.; Markovic, N. M. Measurement of Oxygen Reduction Activities via the Rotating Disc Electrode Method: From Pt Model Surfaces to Carbon-Supported High Surface Area Catalysts. *Electrochim. Acta* **2008**, *53*, 3181−3188.
(40) Shokhen, V.; Zysler, M.; Shviro, M.; Zitoun, D.; Chatenet, M. Carbon-Supported PtNi Nanocrystals for Alkaline Oxygen Reduction and Evolution Reactions: Electrochemical Activity and Durability upon Accelerated Stress Tests. *ACS Appl. Energy Mater.* **2020**, *3*, 8858−8870.
(41) Schalenbach, M.; Kasian, O.; Ledendecker, M.; Speck, F. D.; Mingers, A. M.; Mayrhofer, K. J. J.; Cherevko, S. The Electrochemical Dissolution of Noble Metals in Alkaline Media. *Electrocatalysis* **2018**, *9*, 153−161.
(42) Labata, M. F.; Li, G.; Ocon, J.; Chuang, P.-Y. A. Insights on Platinum-Carbon Catalyst Degradation Mechanism for Oxygen Reduction Reaction in Acidic and Alkaline Media. *J. Power Sources* **2021**, *487*, 229356.
(43) Shinozaki, K.; Zack, J. W.; Pylypenko, S.; Pivovar, B. S.; Kocha, S. S. Oxygen Reduction Reaction Measurements on Platinum Electrocatalysts Utilizing Rotating Disk Electrode Technique: II. Influence of Ink Formulation, Catalyst Layer Uniformity and Thickness. *J. Electrochem. Soc.* **2015**, *162*, F1384.
(44) Mukerjee, S.; Srinivasan, S.; Soriaga, M. P.; McBreen, J. Role of Structural and Electronic Properties of Pt and Pt Alloys on Electrocatalysis of Oxygen Reduction: An in Situ XANES and EXAFS Investigation. *J. Electrochem. Soc.* **1995**, *142*, 1409.
(45) Antolini, E.; Salgado, J. R. C.; Giz, M. J.; Gonzalez, E. R. Effects of Geometric and Electronic Factors on ORR Activity of Carbon Supported Pt−Co Electrocatalysts in PEM Fuel Cells. *Int. J. Hydrogen Energy* **2005**, *30*, 1213−1220.
(46) Toda, T.; Igarashi, H.; Uchida, H.; Watanabe, M. Enhancement of the Electroreduction of Oxygen on Pt Alloys with Fe, Ni, and Co. *J. Electrochem. Soc.* **1999**, *146*, 3750.
(47) García-Contreras, M. A.; Fernández-Valverde, S. M.; Basurto-Sánchez, R. Investigation of Oxygen Reduction in Alkaline Media on Electrocatalysts Prepared by the Mechanical Alloying of Pt, Co, and Ni. *J. Appl. Electrochem.* **2015**, *45*, 1101−1112.
(48) Mukerjee, S.; Srinivasan, S.; Soriaga, M. P.; McBreen, J. Role of Structural and Electronic Properties of Pt and Pt Alloys on Electrocatalysis of Oxygen Reduction. *J. Electrochem. Soc.* **1995**, *142*, 1409.
(49) Song, L.; Liang, Z.; Nagamori, K.; Igarashi, H.; Vukmirovic, M. B.; Adzic, R. R.; Sasaki, K. Enhancing Oxygen Reduction Performance of Pt Monolayer Catalysts by Pd (111) Nanosheets on WNi Substrates. *ACS Catal.* **2020**, *10*, 4290−4298.
(50) Kaito, T.; Tanaka, H.; Mitsumoto, H.; Sugawara, S.; Shinohara, K.; Ariga, H.; Uehara, H.; Takakusagi, S.; Asakura, K. In Situ X-Ray Absorption Fine Structure Analysis of PtCo, PtCu, and PtNi Alloy Electrocatalysts: The Correlation of Enhanced Oxygen Reduction Reaction Activity and Structure. *J. Phys. Chem. C* **2016**, *120*, 11519−11527.
(51) Kuttiyiel, K. A.; Sasaki, K.; Choi, Y.; Su, D.; Liu, P.; Adzic, R. R. Nitride Stabilized PtNi Core−Shell Nanocatalyst for High Oxygen Reduction Activity. *Nano Lett.* **2012**, *12*, 6266−6271.
(52) Krishnadas, K. R.; Sajanlal, P. R.; Pradeep, T. Pristine and Hybrid Nickel Nanowires: Template-, Magnetic Field-, and Surfactant-Free Wet Chemical Synthesis and Raman Studies. *J. Phys. Chem. C* **2011**, *115*, 4483−4490.
(53) Elezović, N. R.; Babić, B. M.; Vračar, L. M.; Krstajić, N. V. Oxygen Reduction at Platinum Nanoparticles Supported on Carbon Cryogel in Alkaline Solution. *J. Serb. Chem. Soc.* **2007**, *72*, 699−708.
(54) Campos-Roldán, C. A.; González-Huerta, R. G.; Alonso-Vante, N. Experimental Protocol for HOR and ORR in Alkaline Electrochemical Measurements. *J. Electrochem. Soc.* **2018**, *165*, J3001−J3007.
(55) Zhang, G.; Yang, D.; Sacher, E. X-Ray Photoelectron Spectroscopic Analysis of Pt Nanoparticles on Highly Oriented Pyrolytic Graphite, Using Symmetric Component Line Shapes. *J. Phys. Chem. C* **2007**, *111*, 565−570.
(56) Ravel, B.; Newville, M. ATHENA, ARTEMIS, HEPHAESTUS: Data Analysis for X-Ray Absorption Spectroscopy Using IFEFFIT. *J. Synchrotron Radiat.* **2005**, *12*, 537−541.
(57) Sasaki, K.; Marinkovic, N.; Isaacs, H. S.; Adzic, R. R. Synchrotron-Based in Situ Characterization of Carbon-Supported Platinum and Platinum Monolayer Electrocatalysts. *ACS Catal.* **2016**, *6*, 69−76.

https://doi.org/10.1021/acsomega.1c00792
ACS Omega 2021, 6, 17203−17216